molecules

MDPI

Article

Phytochemical Investigation of *Carex praecox* Schreb. and ACE-Inhibitory Activity of Oligomer Stilbenes of the Plant

Csilla Zsuzsanna Dávid [1], Norbert Kúsz [1], Orinamhe Godwin Agbadua [1], Róbert Berkecz [2], Annamária Kincses [1,3], Gabriella Spengler [4], Attila Hunyadi [1,3], Judit Hohmann [1,3] and Andrea Vasas [1,3,*]

1 Department of Pharmacognosy, University of Szeged, 6720 Szeged, Hungary; davidzsuzsanna88@gmail.com (C.Z.D.); kusznorbert@gmail.com (N.K.); orinamhe.agbadua@uniben.edu (O.G.A.); kincses.annamaria@szte.hu (A.K.); hunyadi.attila@szte.hu (A.H.); hohmann.judit@szte.hu (J.H.)
2 Institute of Pharmaceutical Analysis, University of Szeged, 6720 Szeged, Hungary; berkecz.robert@szte.hu
3 HUN-REN-USZ Biologically Active Natural Products Research Group, University of Szeged, Eötvös u. 6, 6720 Szeged, Hungary
4 Department of Medical Microbiology, Albert Szent-Györgyi Health Center, Albert Szent-Györgyi Medical School, University of Szeged, 6725 Szeged, Hungary; spengler.gabriella@med.u-szeged.hu
* Correspondence: vasas.andrea@szte.hu

Abstract: Phenolic compounds are the main special metabolites of Cyperaceae species from phytochemical, pharmacological, and chemotaxonomical points of view. The present study focused on the isolation, structure determination, and pharmacological investigation of constituents from *Carex praecox*. Twenty-six compounds, including lignans, stilbenes, flavonoids, megastigmanes, chromenes, and phenylpropanoids, were identified from the methanol extract of the plant. Five of these compounds, namely, carexines A–E, are previously undescribed natural products. All compounds were isolated for the first time from *C. praecox*. The ACE-inhibitory activity of seven stilbenoid compounds was tested, and (–)-hopeaphenol proved to be the most active (IC_{50} 7.7 ± 0.9 μM). The enzyme–kinetic studies revealed a mixed-type inhibition; therefore, domain-specific studies were also conducted. The in silico docking of (–)-hopeaphenol to the ACE affirmed some favorable interactions. In addition, the antiproliferative and antibacterial effects of some compounds were also evaluated.

Keywords: Cyperaceae; *Carex praecox*; lignans; stilbenes; flavonoids; ACE-inhibitory activity

Citation: Dávid, C.Z.; Kúsz, N.; Agbadua, O.G.; Berkecz, R.; Kincses, A.; Spengler, G.; Hunyadi, A.; Hohmann, J.; Vasas, A. Phytochemical Investigation of *Carex praecox* Schreb. and ACE-Inhibitory Activity of Oligomer Stilbenes of the Plant. *Molecules* **2024**, *29*, 3427. https://doi.org/10.3390/molecules29143427

Academic Editors: Iryna Smetanska and Oksana Sytar

Received: 20 June 2024
Revised: 17 July 2024
Accepted: 17 July 2024
Published: 22 July 2024

1. Introduction

Cardiovascular diseases (ischaemic heart disease and stroke) are still the leading causes of death responsible for approximately 27% of the total deaths worldwide [1–3]. The angiotensin I-converting enzyme (ACE), a zinc-dependent dipeptidyl carboxypeptidase, is one of the main targets in treating hypertension, heart failure, myocardial infarction, and other related diseases. The ACE is composed of two independent catalytic domains: The C-domain is mainly responsible for the conversion of angiotensin I to angiotensin II and, thus, regulates blood pressure and hydrolyzing bradykinine, while the N-domain hydrolyzes other peptides, including the hemoregulatory peptide, AcSDKP [4,5]. There are several available inhibitors of the ACE; however, most of them cause unpleasant adverse effects (e.g., dry cough, angioedema). Selective domain inhibitors might have potency in the treatment of hypertension without the undesirable adverse effects and in utilizing the different physiological effects of each ACE domain in clinical use [6].

The *Carex* genus, belonging to the family Cyperaceae (sedges), comprises approximately 2000 species that dominate wetlands, pastures, prairies, tundra, and the herb layer of temperate forests [7]. Sedges are rich sources of phenolic secondary metabolites, like stilbenes, flavonoids, and lignans, but other types of plant metabolites, such as coumarins, quinones, alkaloids, and terpenoids have also been isolated from species of this plant

family [8–11]. However, up to now only a limited number of species (approx. 20) have been investigated from phytochemical and pharmacological points of view [12]. Previous studies revealed that *Carex* species are an abundant source of stilbene-type metabolites, among them monomers, dimers, trimers, and tetramers [12–15]. Cyperaceae stilbenes are mainly oligomers of piceatannol and resveratrol. A 1,2-diaryl-dihydro benzofuran skeleton with *trans*-oriented aryl rings is the most important framework in stilbene oligomers of this family, and it is considered to be biosynthesized by regio- and stereoselective pathways [16]. Stilbenes possess noteworthy biological activities and have been isolated from other heterogeneous and phylogenetically unrelated plant families, e.g., Dipterocarpaceae, Gnetaceae, Leguminosae, Polygonaceae, and Vitaceae, etc. [12,17]. Our study aimed to isolate and identify specialized metabolites, especially stilbenes, from *Carex praecox*. *C. praecox* Schreb. (early sedge, spring sedge) is a perennial, 8–30 cm plant native to Europe and western Asia and is commonly found in moist to wet habitats, forests, or mountain grasslands. There is no available information on the ethnomedicinal importance of *C. praecox* and, according to the literature, it has not been investigated either from phytochemical or pharmacological points of view.

We describe here the isolation and structure determination of carexins A–E (**1**–**5**) and the identification of 21 other compounds (**6**–**26**), among them lignans, flavonoids, stilbenes, and megastigmanes, as well as the ACE-inhibitory activity of the isolated stilbenes.

2. Results

2.1. Isolation and Structure Determination of the Compounds

Dried and ground *C. praecox* plant material was extracted with methanol at room temperature. After evaporation, the extract was dissolved in 50% aqueous methanol and subjected to solvent–solvent partitioning with *n*-hexane, chloroform, and ethyl acetate. Both the chloroform and the ethyl acetate phases of the plant were further purified by different chromatographic techniques, including column chromatography (CC), vacuum liquid chromatography (VLC), flash chromatography (FC), rotational planar chromatography (RCP), preparative thin-layer chromatography (TLC), and HPLC to afford altogether 26 compounds, among them 5 previously undescribed natural products (carexines A–E, **1**–**5**) (Figure 1).

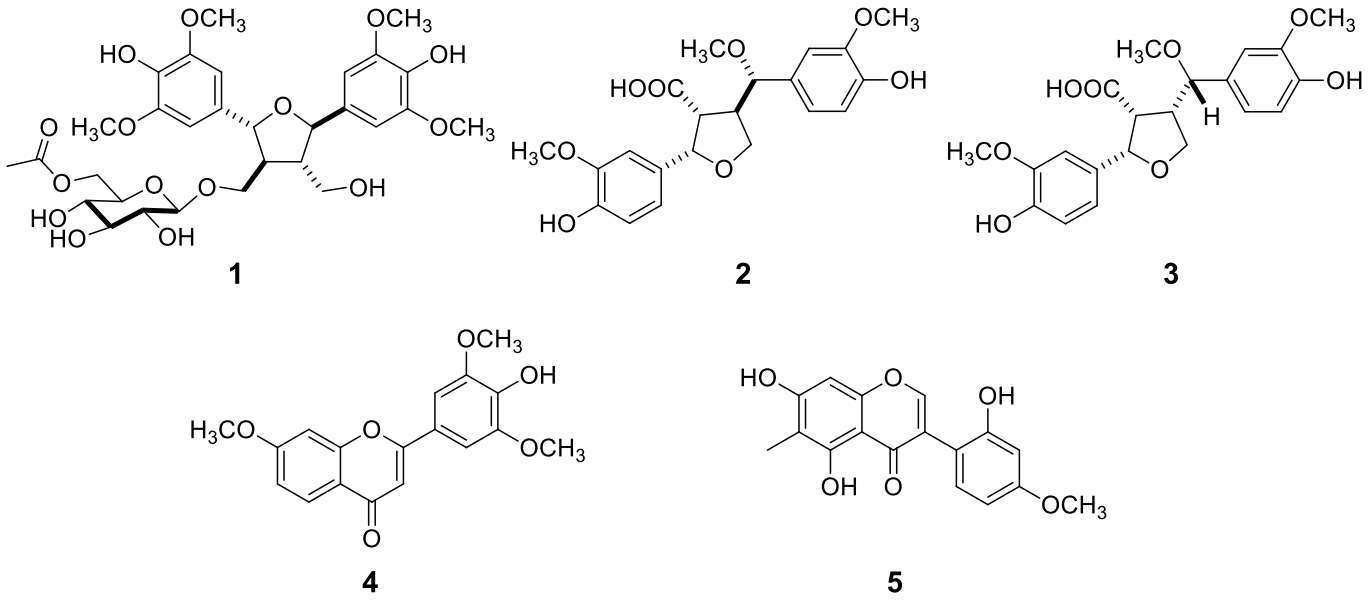

Figure 1. Structures of carexines A–E (**1**–**5**).

The structure elucidation of the isolated compounds was carried out by extensive spectroscopic analysis, applying 1D (^{1}H and JMOD) and 2D (^{1}H–^{1}H COSY, HSQC, HMBC,

and NOESY) NMR and HRMS measurements, and a comparison of the spectral data with the values in the literature.

Compound **1** was isolated as yellowish oil and exhibited a brownish-purple color on the TLC plate by spraying with vanillin sulfuric acid and then heating. The molecular formula was determined as $C_{30}H_{40}O_{15}$ from molecular ion peaks $[M + NH_4]^+$ at *m/z* 658.2711 (calcd for $C_{30}H_{44}NO_{15}^+$ 658.2711) and $[M + Na]^+$ *m/z* 663.2258 (calcd for $C_{30}H_{40}O_{15}Na^+$ 663.2264) in the HRESIMS. The ^{1}H NMR spectrum displayed signals due to four aromatic protons [δ_H 6.74 (2H, s, H-2, H-6), 6.71 (2H, s, H-2′, H-6′)]; two methines [δ_H 2.44 (1H, m, H-8), 2.32 (1H, m, H-8′)]; two oxymethylenes [δ_H 3.96 (1H, dd, *J* = 10.1, 5.0 Hz, H-9a), 3.65 (1H, dd, *J* = 10.1, 5.0 Hz, H-9b), 3.71 (1H, dd, *J* = 11.6, 4.4 Hz, H-9′a), 3.59 (1H, dd, *J* = 11.6, 4.4 Hz, H-9′b)]; two oxymethines [δ_H 5.05 (1H, d, *J* = 8.4 Hz, H-7), 4.98 (1H, d, *J* = 8.5 Hz, H-7′)]; four methoxy groups [δ_H 3.83 (12H, s, CH_3O-3, CH_3O-5, CH_3O-3′, CH_3O-5′)]; one methyl group [δ_H 1.94 (3H), s]; and an anomeric proton [δ_H 4.25 (1H, d, *J* = 7.9 Hz, H-1″)] (Table 1). The ^{13}C NMR spectrum showed signals due to a glucopyranosyl group [δ_C 64.6 (C-6″), 71.6 (C-4″), 75.1 (C-2″), 78.0 (C-3″), 75.3 (C-5″), 104.7 (C-1″)]; one methyl group (δ_C 20.6); and a carbonyl group (δ_C 172.7). The relatively large $^3J_{1''-2''}$ value (7.8 Hz) of the anomeric proton of this glucopyranosyl group indicated a *β*-orientation.

Table 1. ^{1}H (500 MHz) and ^{13}C (125 MHz) NMR Data of Compound **1**.

Position	^{1}H	^{13}C	Position	^{1}H	^{13}C
	δ_H (ppm), *J* (Hz)	δ_C, Type		δ_H (ppm), *J* (Hz)	δ_C, Type
1		134.3, C	1′		134.3, C
2,6	6.74 s	104.9, CH	2′,6′	6.71 s	104.9, CH
3		149.3, C	3′		149.3, C
4		136.1, * C	4′		136.2, * C
5		149.3, C	5′		149.3, C
7	5.05 d (8.4)	84.6, CH	7′	4.98 d (8.5)	84.3, CH
8	2.44 m	51.9, CH	8′	2.32 m	54.5, CH
9	3.96 dd (10.1, 5.0), 3.65 dd (10.1, 5.0)	69.9, CH_2	9′	3.71 dd (11.6, 4.4), 3.59 dd (11.6, 4.4)	61.0, CH_2
1″	4.25 d (7.9)	104.7, CH			
2″	3.16 br t (7.9)	75.1, CH			
3″	3.30 m	78.0, CH			
4″	3.25 m	71.6, CH			
5″	3.41 m	75.3, CH			
6″	4.33 dd (11.9, 2.1), 4.15 dd (11.9, 5.8)	64.6, CH_2			
3/3′-OCH_3	3.83 s	56.9, CH_3			
5/5′-OCH_3	3.83 s	56.9, CH_3			
Ac-CO		172.7, C			
Ac-Me	1.94 s	20.6, CH_3			

* interchangeable signals.

From these data, the aglycone suggested a 2,5-diaryl-tetrahydrofuranoid-type lignan, and based on the comparison of its NMR data with the literature values, it was identified as icariol A_2 [18]. HMBC spectrum determined the position of the *β*-D-glucopyranosyl group to be at C-9 by showing correlations between the anomeric proton (δ_H 4.25) and C-9 (δ_C 69.9) of the aglycone, as shown in Figure 2. This derivative is also known in nature [19]. Moreover, the HMBC between the methyl protons (δ_H 1.94) and methylene protons of H_2-6″ (δ_H 4.33 and 4.15) with carbonyl carbon (δ_C 172.7) determined that the glucose moiety was acetylated at C-6″.

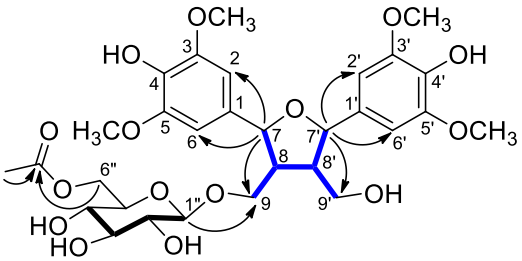

Figure 2. Diagnostic ^{1}H–^{1}H COSY (—) and HMBCs (H → C) of compound **1**.

The NOESY correlations confirmed the position of the *β*-D-glucopyranosyl group to be at C-9 by showing correlations between H-1″ and H-9a and H-9b. The NOESY correlations were detected between H-7 and H-9a/9b and H-7′ and H-9′a/9′b, proving H-7 to be on the same side as 9-methylene, and H-7′ on the same side as 9′-methylene. This is in agreement with the coupling constants of H-7 ($J_{7,8}$ = 8.4 Hz) and H-7′ ($J_{7',8'}$ = 8.5 Hz) in *trans* position with H-8 and H-8′, respectively. Thus, the structure of **1** was assigned as icariol A_2 9-*O*-*β*-D-(6″-acetyl)-glucopyranoside, a new natural compound, and named carexine A (Figure 1).

The molecular formula of carexine B (**2**) was determined as $C_{21}H_{24}O_8$ from a molecular ion peak at *m/z* 403.1443 $[M - H]^-$ (calcd for $C_{21}H_{23}O_8^-$ 403.1441) in the HRESIMS. The ^{1}H NMR spectrum of compound **2** displayed six olefin methine proton signals at δ_H 6.91 (1H, d, *J* = 1.8 Hz, H-2); 6.78 (1H, d, *J* = 8.1 Hz, H-5); 6.77 (1H, dd, *J* = 8.1, 1.8 Hz, H-6); 6.92 (1H, d, *J* = 1.8 Hz, H-2′); 6.80 (1H, d, *J* = 8.0 Hz, H-5′); and 6.78 (1H, dd, *J* = 8.0, 1.8 Hz, H-6′) due to two 1,3,4-trisubstituted benzene rings (Table 2). The proton signals at δ_H 5.07 (1H, d, *J* = 7.2 Hz, H-7) and 4.26 (1H, d, *J* = 10.4 Hz, H-7′) were interpreted as two oxygenated methines, and the proton signals at δ_H 3.63 (1H, t, *J* = 8.6, 7.6 Hz, H-9′a) and 3.56 (1H, t, *J* = 8.6 Hz, H-9′b) were due to an oxygenated methylene showing geminal (^{2}J) coupling. Moreover, the proton signals at δ_H 3.84, 3.87, and 3.06 (3 × 3H, s) indicated the presence of three methoxy groups in the molecule. The remaining proton signals at δ_H 3.07 (1H, m, H-8) and 3.00 (1H, m, H-8′) were determined as two methines, suggesting the presence of a furanolignan skeleton. In the JMOD spectrum, 18 carbon signals, including a carboxyl group [δ_C 176.6 (C-9)] were observed, confirming **2** to be a lignan substituted with three methoxy (δ_C 2 × 56.4 and 56.0) and two hydroxyl groups. The partial structures of compound **2** were determined by a ^{1}H–^{1}H COSY experiment (Figure 3). Correlations were observed between δ_H 3.00 (H-8′), with the oxygenated methylene proton signals at δ_H 3.63 (H-9′a) and 3.56 (H-9′b), and the methine proton signals at δ_H 3.07 (H-8) and δ_H 4.26 (H-7′). Moreover, δ_H 3.07 (H-8) correlated with δ_H 5.07 (H-7). The location of the phenyl, methoxy, and carboxyl groups of compound **2** was determined by the HMBC experiment (Figure 3). HMBCs were observed between the methine proton signal H-7′, with the aromatic methine carbon signals at δ_C 121.5 (C-6′) and 111.4 (C-2′), methoxy carbon signal at δ_C 56.0 (OCH_3-7′) and methine signal at δ_C 51.2 (C-8′). The methine proton signal H-8 showed a correlation with the carboxy carbonyl signal at δ_C 176.6 (C-9) and the quaternary carbon signal at δ_C 133.9 (C-1). Finally, diagnostic HMBCs were observed between H-7 and aromatic ring signals at δ_C 110.6 (C-2) and 119.7 (C-6). Therefore, the structure of compound **2** was determined to be 8-carboxyl-4,4′-dihydroxy-3,3′,7′ trimethoxy-7,9′-epoxy-8,8′-lignan, and named carexine B.

In the NOESY spectrum, the cross peaks between H-7/H-8, H-7/H-9′b, H-7/H-7′, and H-7′/H-9′b indicated the *β*-configuration of these protons, while the NOE correlation between H-9′a and H-8′ indicated the *α*-configuration of H-9′a and H-8′ (Figure 4).

Table 2. ^{1}H (500 MHz) and ^{13}C (125 MHz) NMR Data of Compounds **2** and **3**.

	2		**3**	
Position	**^{1}H**	**^{13}C**	**^{1}H**	**^{13}C**
	δ_H (ppm), *J* (Hz)	**δ_C, Type**	**δ_H (ppm), *J* (Hz)**	**δ_C, Type**
1	-	133.9, C	-	134.9, C
2	6.91 d (1.8)	110.6, CH	6.90 d (1.6)	110.6, CH
3	-	149.1, C	-	148.9, C
4	-	147.9, * C	-	147.1, C
5	6.78 d (8.1)	116.1, CH	6.77 d (8.1)	116.2, CH
6	6.77 dd (8.1, 1.8)	119.7, CH	6.78 dd (8.1, 1.6)	119.6, CH
7	5.07 d (7.2)	86.0, CH	5.12 d (5.9)	85.5, CH
8	3.07 m	56.4, CH	2.72 dd (8.4, 5.9)	56.4, CH
9	-	176.6, C	-	176.8, C
1′	-	132.8, C	-	132.9, C
2′	6.92 d (1.8)	111.4, CH	6.85 d (1.6)	111.7, CH
3′	-	149.4, C	-	149.1, C
4′	-	147.4, * C	-	147.3, C
5′	6.80 d (8.0)	116.1, CH	6.73 d (8.1)	116.0, CH
6′	6.78 dd (8.0, 1.8)	121.5, CH	6.76 dd (8.1, 1.6)	121.0, CH
7′	4.26 d (10.4)	83.6, CH	4.51 d (7.1)	83.3, CH
8′	3.00 m	51.2, CH	2.90 m	50.3, CH
9′a (α)	3.63 t (8.6, 7.6)	71.4, CH_2	4.15 d (7.9) 2H	71.6, CH_2
9′b (β)	3.56 t (8.6)			
3-OCH_3	3.84 s	56.4, CH_3	3.80 s	56.4, CH_3
3′-OCH_3	3.87 s	56.4, CH_3	3.84 s	56.4, CH_3
7′-OCH_3	3.06 s	56.0, CH_3	3.15 s	56.6, CH_3

* interchangeable signals.

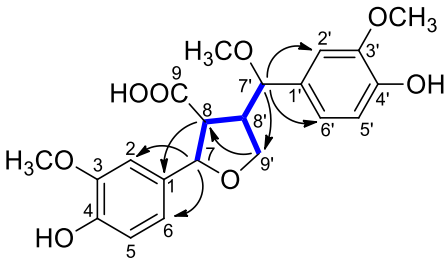

Figure 3. Diagnostic ^{1}H-^{1}H COSY (—) and HMBCs (H → C) of compound **2**.

2 **3**

Figure 4. Key NOESY correlations (⟷) of compounds **2** and **3**.

The molecular formula and molecular weight of carexine C (**3**) were found to be the same as those of compound 2, based on the HRESIMS data. Only slight differences could be observed in the 1D and 2D NMR spectra (Table 2). The only difference between the

two compounds was the *cis* orientation of H-8/H-8′, as shown by the NOESY correlation between H-8′ and H-8 and H-8′ and H-7 (Figure 4). Previously, a lignan (vibruresinol) with the same skeleton was reported from the stems of *Viburnum erosum* [20].

Carexine D (**4**) was obtained as a pale yellow amorphous powder, and its molecular formula was established as $C_{18}H_{16}O_6$ from the HRESIMS peak at *m/z* 329.1018 $[M + H]^+$ (calcd for $C_{18}H_{17}O_6$, 329.1020). The ^{1}H NMR spectrum of **4** exhibited six aromatic proton signals, among them an ABX system at δ_H 8.04 (1H, d, *J* = 8.9 Hz, H-5); 7.07 (1H, dd, *J* = 8.9, 2.4 Hz, H-6); 7.28 (1H, d, *J* = 2.4 Hz, H-8)]; two singlet protons at δ_H 7.33 (2H, s, H-2′, H-6′); and one methine proton [δ_H 6.78 (1H, s, H-3)]. Besides the aromatic protons, signals of three methoxy groups at δ_H 3.98 (3H, OCH_3) and 3.97 (6H, 2 × OCH_3) could be detected. In the JMOD spectrum, signals assigned to a 15-carbon-containing flavonoid skeleton were detected (Table 3). The aromatic singlet at δ_H 6.78 was assigned to H-3 as it showed an HMBC with C-10 (δ_C 118.2), C-2 (δ_C 166.1), and C-1′ (δ_C 123.0) (Figure 5). The three methoxy groups were assigned to be attached to C-7, C-3′, and C-5′, which were determined by HMBC cross-peaks from δ_H 3.98 to δ_C 166.4 (C-7), and δ_H 3.97 to δ_C 149.8 (C-3′ and C-5′). The connection of ring B to ring C was proved by the HMBC correlation detected between H-2′,6′, and C-2. Interestingly, ring A is substituted only with a methoxy group at C-7. Hence, compound **4** was determined as 4′-hydroxy-7,3′,5′-trimethoxyflavone, a new flavonoid named carexine D.

Table 3. ^{1}H (500 MHz) and ^{13}C (125 MHz) NMR Data of Compounds **4** and **5**.

	4		**5**	
Position	**^{1}H**	**^{13}C**	**^{1}H**	**^{13}C**
	δ_H (ppm), *J* (Hz)	**δ_C, Type**	**δ_H (ppm), *J* (Hz)**	**δ_C, Type**
2		166.1, C	8.00 s	156.5, C
3	6.78 s	106.1, CH		122.3, C
4		180.2, C		182.6, C
5	8.04 d (8.9)	127.5, C		160.5, C
6	7.07 dd (8.9, 2.4)	116.1, CH		109.1, C
7		166.4, C		164.0, C
8	7.28 d (2.4)	101.7, CH	6.41 s	93.8, CH
9		159.7, C		157.5, C
10		118.2		105.9, C
11	-	-	2.07 s	7.4, CH_3
1′		123.0, C		112.3, C
2′	7.33 s	105.5, CH		157.8, C
3′		149.8, C	6.48 br s	103.1, CH
4′		141.2, CH		162.7, C
5′		149.8, C	6.49 dd (8.3, 2.5)	106.6, CH
6′	7.33 s	105.5, CH_2	7.13 d (8.3)	133.2, CH
7-OCH_3	3.98 s	56.7, CH_3		
3′-OCH_3	3.97 s	57.2, CH_3		
4′-OCH_3			3.78 s	55.7, CH_3
5′-OCH_3	3.97 s	57.2, CH_3		

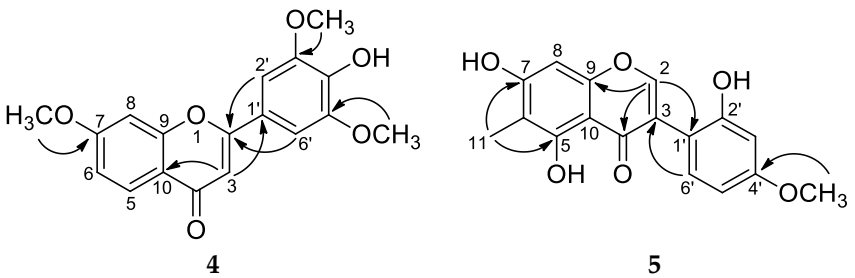

4 **5**

Figure 5. Diagnostic HMBCs (H → C) of compounds **4** and **5**.

Carexine E (**5**) has the molecular formula $C_{17}H_{14}O_6$ compatible with the protonated molecular peak at *m/z* 315.0865 $[M + H]^+$ (calcd for $C_{17}H_{15}O_6^+$ 315.0869) in the HRESIMS. In the ^{1}H NMR spectrum, five aromatic proton signals at δ_H 8.00 (1H, s, H-2); 7.13 (1H, d, *J* = 8.3 Hz, H-6′); 6.49 (1H, dd, *J* = 8.3, 2.5 Hz, H-5′); 6.48 (1H, br s, H-3′) and 6.41 (1H, s, H-8); one methoxy signal at δ_H 3.78 (3H, s, CH_3O-4′); and one methyl signal (δ_H 2.07, s, CH_3-11) were detected. The isoflavone nature of **5** was evident from the H-2 chemical shift of the singlet at δ_H 8.00 and from HMBCs detected between H-2 and C-9, C-4, and C-1′ and between H-6′ and C-3. Based on the ^{1}H NMR and JMOD spectra, compound **5** is a penta-substituted isoflavone. The position of the substituents was determined by HMBC measurement, long-range correlations were observed between CH_3-11 and C-5, C-6, and C-7 and between OCH_3-4′ and C-4′, proving that the methyl group is joined at C-6, and the methoxy group is attached to C-4′. Therefore, compound **5** was determined as 5,7,2′-trihydroxy-4′-methoxy-6-methylisoflavone and named carexine E.

Besides the new compounds carexines A–E (**1**–**5**), 21 known compounds were also isolated from *C. praecox*. The structural characterization was performed through HRESIMS, 1D, and 2D NMR experiments and then by comparison of the ^{1}H and ^{13}C assignations with reported literature data. All compounds were isolated for the first time from this plant. The compounds were identified as two known lignans [4-ketopinoresinol **6**) [21] and (+)-pinoresinol (**7**)] [22], three flavonoids [chrysosplenol F (**8**) [23], tricin (**9**) [24], quercetin (**10**) [25], the chalcone cilicicone b (**11**) [26], seven stilbenes [*trans*-resveratrol (**12**) [27], *cis*-ε-viniferin (**13**) [28], *trans*-ε-viniferin (**14**) [28], *Z*-miyabenol C (**15**) [29], (–)-hopeaphenol (**16**) [30], kobophenol A (**17**) [29], carexinol A (**18**) [15], two megastigmanes, namely, (*S*)-(+)-dehydrovomifoliol (**19**) [31] and 5α,6α-epoxy-3β-hydroxy-7-megastimen-9-one (**20**) [32], two chromones [7-hydroxychromone (**21**) [33] and 5,7-dihydroxychromone (**22**) [34], and other phenolic compounds [vanillin (**23**) [35], *p*-hydroxybenzaldehyde (**24**), piceol (**25**) [36], and vanillic acid (**26**) [35] (Figure 6). Previously unpublished ^{1}H and ^{13}C NMR data of compound **8** (chrysosplenol F) and ^{1}H NMR data of **9** in methanol are given in the experimental section.

Based on the isolated compounds, the main constituents of *C. praecox* are stilbenoids. Among the stilbenoids, monomers [*trans*-resveratrol (**12**)], dimers [*cis*- and *trans*-ε-viniferin (**13**, **14**)], trimers [*Z*-miyabenol C (**15**)], tetramers [(–)-hopeaphenol (**16**), kobophenol A (**17**), and carexinol A (**18**)] were identified. Compounds **12**, **13**, **15**, **17,** and **18** were isolated previously from other Cyperaceae species [12]. The lignans identified from *C. praecox* are tetrahydrofuranoid-type ones. The chromones are known as flavonoid degradation products.

According to our phytochemical results, *C. praecox* is a rich source of polyphenolic compounds. Polyphenols, including flavonoids, stilbenes, phenolic acids, lignans, and others, possess different health benefits [37]. They are secondary plant metabolites implicated in protection against pathogens and ultraviolet radiation and have allelopathic effects [38]. Due to their known antioxidant activity, they have been attributed a probable role in preventing various diseases associated with oxidative stress, such as cancer and cardiovascular and neurodegenerative diseases [39]. It is hypothesized that the increasing concentration of complex stilbenes often occurs in response to plant stresses (via unknown mechanisms) and potentially enhances antioxidant activity and antifungal capacities [40].

Megastigmanes are identified as phytotoxic compounds. Several compounds inhibited the germination of *Lactuca sativa* seeds [41], e.g., 5,7-dihydroxy chromone (**22**) inhibited the germination of velvetleaf seeds; therefore, it has allelopathic activity [42]. *p*-Cresol (**25**) also possessed an allelopathic effect [43]. Tricin (**9**) has been previously isolated from other Cyperaceae species, such as *Cyperus exaltatus* var. *iwasakii* [44], *Rhynchospora corymbose* [45], and *Cyperus rotundus* [46]. Tricin (**9**) exerts unique biological activities over other flavonoids, such as antileishmanial [47], and antihistaminic [48] effects, and has a protective effect against UV-B-irradiation-caused skin damage [49].

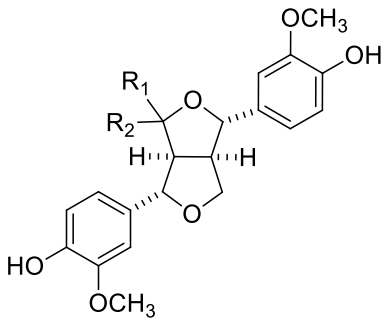

	R_1	R_2
6	=O	
7	H	H

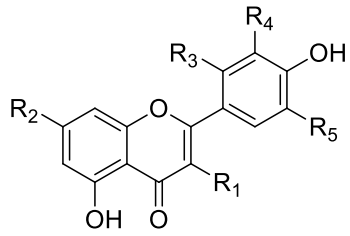

	R_1	R_2	R_3	R_4	R_5
8	OCH_3	OCH_3	OH	H	OCH_3
9	H	OH	H	OCH_3	OCH_3
10	OH	OH	H	H	OH

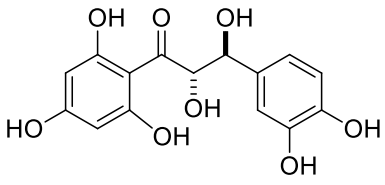

11

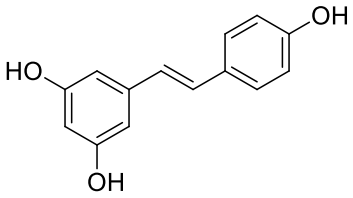

12

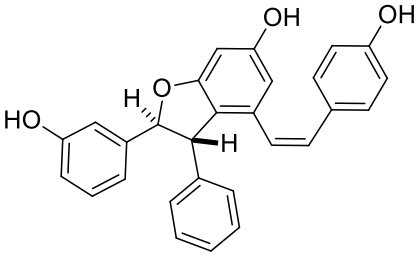

13

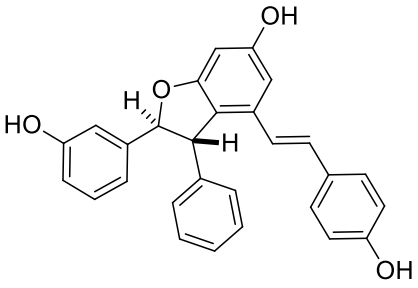

14

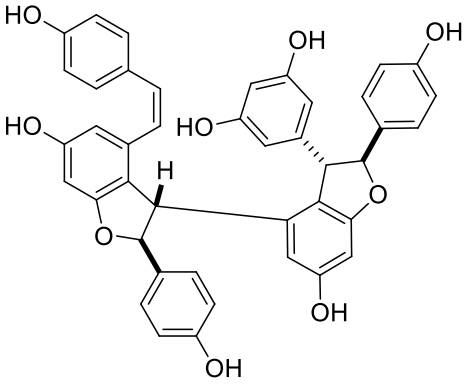

15

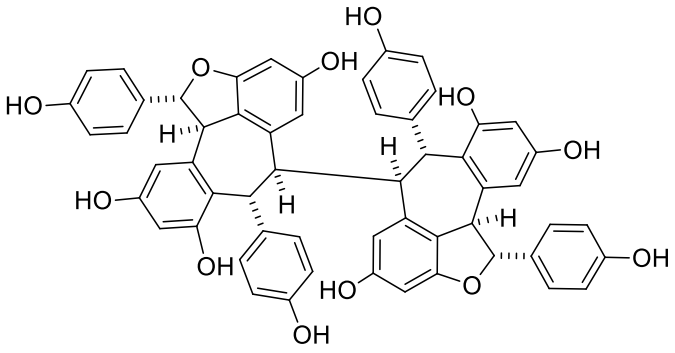

16

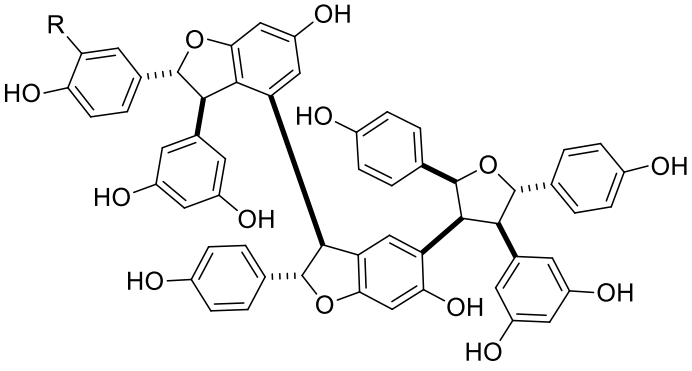

	R
17	H
18	OH

Figure 6. *Cont.*

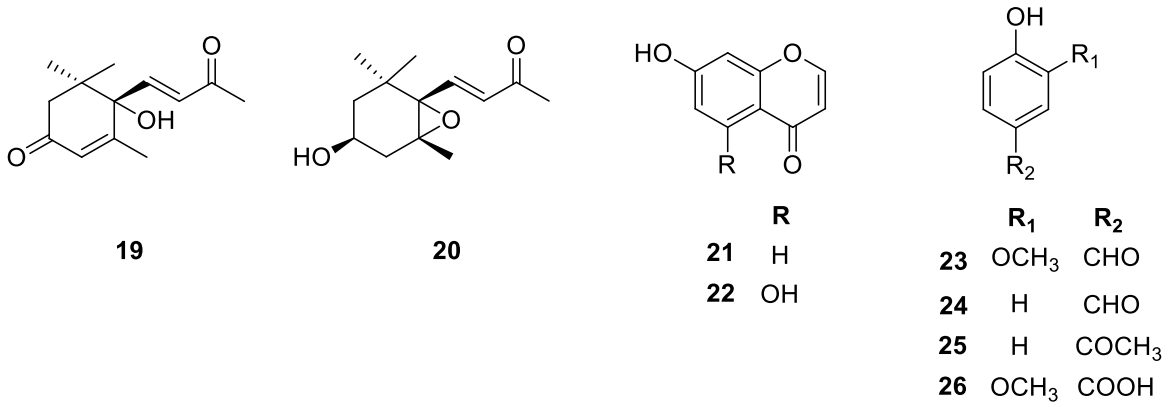

Figure 6. Structures of other compounds (**6**–**26**) isolated from *C. praecox*.

Hopeaphenol (**16**) was the first oligostilbene to be isolated in 1951 from *Hopea odorata* (Dipterocarpaceae) [50]. (–)-Hopeaphenol (**16**), was identified as a selective inhibitor of HIV transcription that targets, in part, PKC- and NF-κB-mediated HIV transcription and CDK9 activity in T cells, resulting in the inhibition of virus production in vitro and infectious virus replication in peripheral blood mononuclear cells (PBMCs) [51]. The compound also inhibited cellular entry of SARS-CoV-2 USA-WA1/2020, B.1.1.7, and B.1.351 variants [52].

2.2. Pharmacological Assays

The isolated stilbenes (**12**–**18**) were subjected to different pharmacological studies. To investigate the potential cardioprotective effect of the isolated stilbenes, an ACE-inhibitory assay was performed, and the IC_{50} values of the compounds were determined. All the tested stilbenes (except resveratrol (**12**)) exerted notable activity at a concentration of 90 μM; among them, the tetramer (–)-hopeaphenol (**16**) was the most active, with an IC_{50} value of 7.7 ± 0.9 μM (Table 4).

Table 4. Results of the ACE-inhibitory assay.

Compound	Inhibition at 90 μM (%) ± SD	IC_{50} (μM) ± SD
12	35.4 ± 3.9	185.8 ± 12.8
13	95.5 ± 2.8	18.0 ± 1.2
14	106.7 ± 1.1	14.0 ± 0.7
15	96.7 ± 6.3	15.2 ± 0.4
16	102.8 ± 1.5	7.7 ± 0.9
17	98.5 ± 1.2	14.8 ± 0.8
18	98.7 ± 3.8	22.3 ± 0.9
Captopril	80.8 ± 1.2	0.2 ± 0.1

For a better understanding of the actual interaction between (–)-hopeaphenol (**16**) and the ACE, a domain-specific assay was performed. The inhibitory activity of compound **16** compared to bradykinin-potentiating peptide b (BPPb) on the C- and N-domain of a rabbit lung ACE using the FRET substrates was investigated. Based on the results, (–)-hopeaphenol (**16**) inhibits the N-domain favorably (IC_{50} = 35.67 ± 2.3 μM), while it has a 10 times lower affinity for the C-domain (IC_{50} > 300 μM) (Table 5).

Since selective inhibition of the N-domain will result in the accumulation of AcSDKP, it might be promising for treating fibrosis without affecting blood pressure [53]. Furthermore, inhibition of the N-terminal ACE-active site may have important clinical applications in facilitating hematopoietic recovery after aggressive cancer chemotherapy by controlling the hematopoietic cycle and stem cell proliferation [54].

Table 5. Domain-specific inhibitory capacity of (–)-hopeaphenol (**16**) compared to BPPb (substrate concentration [S] = KM calculated from initial velocity studies of both substrates; Abz-SDK(Dnp)P-OH; [S] = 72 μM and Abz-LFK(Dnp)-OH; [S] = 21 μM).

	Inhibition (%) ± SD	
	N-Domain	**C-Domain**
BPPb (200 nM)	5.2 ± 0.2	83.20 ± 3.6
16 (10 μM)	42.41 ± 0.8	18.17 ± 0.5
16 (50 μM)	55.74 ± 3.2	23.39 ± 0.6

2.3. Molecular Docking

In silico docking was applied to characterize the binding behavior of (–)-hopeaphenol (**16**). The energy-minimized model of compound (**16**) was docked using AutoDock4 into both domains of the ACE crystal structure retrieved from the Protein Data Bank (PDB ID: 1O86 for the C-domain and 2C6N for the N-domain) to explain the chemical interactions between (–)-hopeaphenol (**16**) and both ACE active binding sites. This program uses the Lamarckian genetic algorithm (LGA) to generate a range of potential conformations from a starting ligand in an arbitrary conformation and then searches for favorable dockings at the protein-binding site [55]. The docking results revealed a network of hydrogen bonds and electrostatic and hydrophobic interactions between (–)-hopeaphenol (**16**) and the N-domain of the ACE with a strong binding energy (E = −9.83 kcal/mol). Importantly, interaction with residues Tyr^{369}, Arg^{381}, and Thr^{496} could be detected; these residues were previously connected to the N-domain selectivity [56]. The most important interactions are the π–π interactions between (–)-hopeaphenol (**16**) and Tyr^{369} and the carbon–hydrogen bond with Arg^{381} (Figure 7).

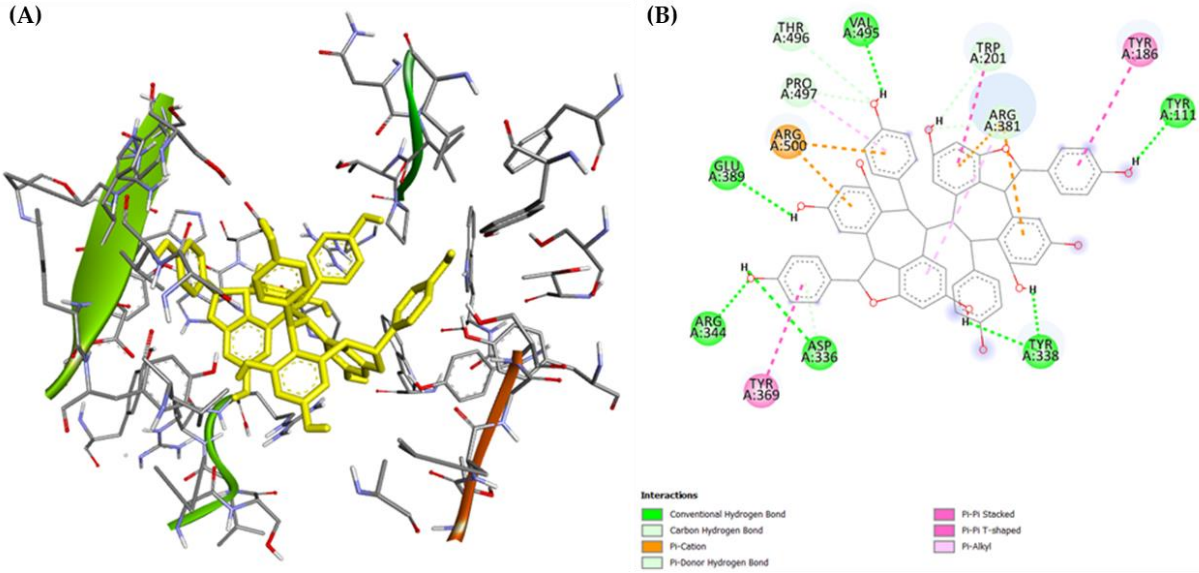

Figure 7. Binding of (–)-hopeaphenol (**16**) to the N-domain. (**A**): 3-D interactions of (–)-hopeaphenol (**16**) in yellow, with the active site amino acids. (**B**): 2-D interaction showing the type of bonding interactions with the active site residues.

On the other hand, (–)-hopeaphenol (**16**) bound to the C-domain with a very poor affinity (binding energy: E = +41.42 kcal/mol). Several unfavorable interactions were identified as the reason for the low binding efficiency (Figure 8). This is well in line with the results of the in vitro domain-specific studies, suggesting that (–)-hopeaphenol (**16**) is an N-domain-selective ACE inhibitor.

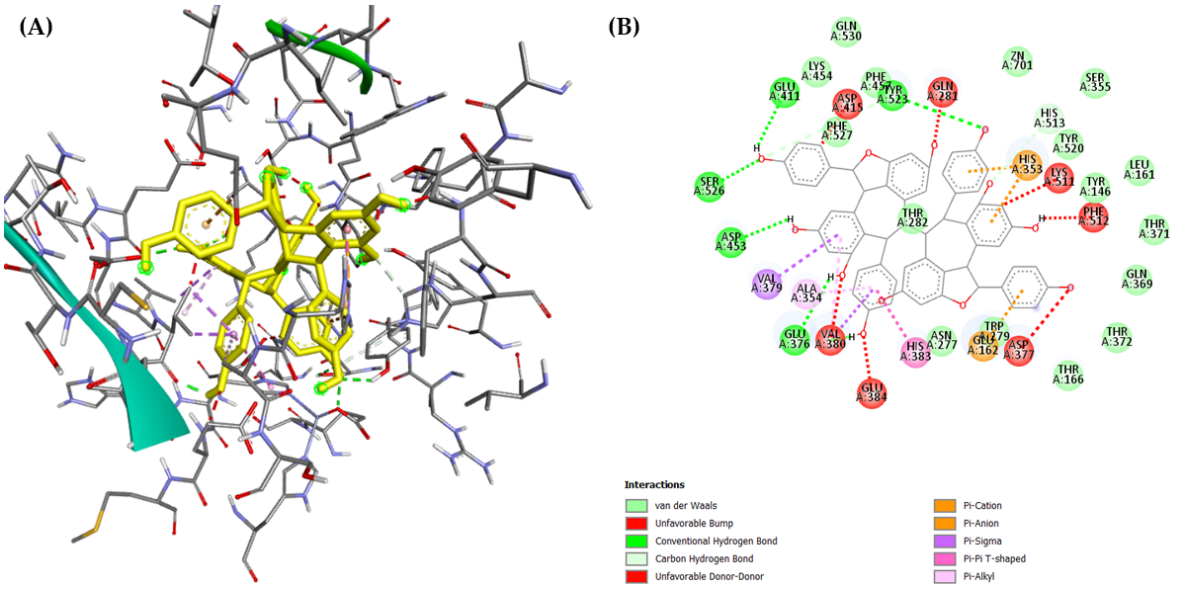

Figure 8. Binding of (–)-hopeaphenol (**16**) to the C-domain. (**A**): 3-D interactions of (–)-hopeaphenol (**16**) in yellow, with the active site amino acid residues. (**B**): 2-D interaction showing the type of bonding interactions, with several unfavorable interactions observed.

2.4. Other Pharmacological Assays

The antiproliferative capacity of compounds **12**–**18** was tested against human colon adenocarcinoma cells (Colo 205 sensitive and the resistant Colo 320/MDR-LRP expressing ABCB1). A thiazolyl blue tetrazolium bromide (MTT) assay was used for each compound to assess the concentration required for 50% inhibition of viability of the cell population (IC_{50}), and cisplatin and doxorubicin were used as positive controls. Interestingly, only the monomer resveratrol (**12**) and the tetramer (–)-hopeaphenol (**16**) exerted notable antiproliferative activity against both cell lines with IC_{50} values comparable to those of the two positive controls, while the other stilbenes were found inactive (Table 6).

Table 6. Results of the antiproliferative assay (IC_{50} in μM ± SD).

	Colo 205	Colo 320
Compound	**IC_{50} (μM) ± SD**	**IC_{50} (μM) ± SD**
12	48.33 ± 1.54	40.4 ± 1.84
13	>100	>100
14	>100	>100
15	>100	>100
16	1.59 ± 0.11	6.08 ± 0.24
17	>100	>100
18	>100	>100
DMSO	>1%	>1%
Cisplatin	53.93 ± 3.92	64.68 ± 3.56
Doxorubicin	0.33 ± 0.03	0.67 ± 0.06

The antibacterial effect of the *n*-hexane, chloroform, and ethyl acetate fractions of the methanol extract of *C. praecox* was investigated against *Bacillus subtilis*, *Escherichia coli*, *Klebsiella pneumoniae*, *Moraxella catarrhalis*, MRSA, *Pseudomonas aeruginosa*, *Staphylococcus aureus*, *S. epidermidis*, and *Streptococcus pyogenes* using the disk diffusion method. The ethyl acetate fraction showed remarkable activity against *S. epidermidis* (inhibitory zone 18 mm), *S. aureus* (14 mm), MRSA (14 mm), *M. catarrhalis* (9 mm), and *B. subtilis* (12 mm), respectively. Therefore, the antibacterial effect of the isolated stilbenes (**12**–**18**) was also in-

vestigated against these bacterial strains, but none of the compounds possessed remarkable antibacterial activity (data not indicated).

3. Materials and Methods

3.1. General Experimental Procedures

NMR spectra were recorded in methanol-d_4, chloroform ($CDCl_3$), and DMSO-d_6 on a Bruker Avance DRX 500 spectrometer (Bruker, Ettlingen, Germany) at 500 MHz (^{1}H) and 125 MHz (^{13}C). The signals of the deuterated solvents were chosen as references. The chemical shift values (δ) were given in ppm, and the coupling constants (J) are in Hz. The two-dimensional (2D) experiments were conducted using standard TopSpin 3.6.1 Bruker software. Gradient-enhanced versions were applied in correlation spectroscopy (^{1}H–^{1}H COSY), nuclear Overhauser effect spectroscopy (NOESY), heteronuclear single quantum coherence spectroscopy (HSQC), and heteronuclear multiple bond correlation (HMBC) experiments. The high-resolution MS spectra were acquired with a Thermo Scientific Q-Exactive Plus Orbitrap mass spectrometer (Thermo Fisher Scientific, Waltham, MA, USA) equipped with an ESI ion source in positive ionization mode. The data were acquired and processed with MassLynx software 4.1 (SCN805). Optical rotation measurements were carried out by a Jasco-P2000 digital polarimeter (JASCO Corporation, Tokyo, Japan).

The normal and reversed-phase vacuum liquid chromatography (VLC) were carried out on a silica gel (Kieselgel 60 GF_{254}, 15 μm, Merck, Darmstadt, Germany) and on a reversed-phase silica gel [RediSep C-18, 40–60 μm, Teledyne Isco, Lincoln, NE, USA]. The thin-layer chromatography was performed on Kieselgel 60 RP-18 F_{254} and Kieselgel 60 F_{254} (Merck, Darmstadt, Germany). The TLC plates were detected under a UV light at 254 nm and by spraying with a vanillin–sulfuric acid reagent, followed by heating. The flash chromatography (FC) was processed with a Combi Flash Rf^+ Lumen instrument (Teledyne Isco) on a reversed-phase RediSep Rf HP Gold (50 g) column. Sephadex LH-20 (25–100 μm, Sigma-Aldrich, St. Louis, MO, USA) was used for gel filtration. The rotation planar chromatography (RPC) was carried out using a Chromatotron instrument (Model 8924, Harrison Research, T-Squared Technology, Inc., San Bruno, CA, USA). The high-performance liquid chromatographic (HPLC) separation was carried out on a Waters HPLC (Waters 600 controller, Waters 600 pump, and Waters 2998 photodiode array detector, Waters, Milford, MA, USA) and a Shimadzu HPLC (Shimadzu LC40, Shimadzu, Tokyo, Japan) using normal phase [LiChrospher Si 100 (250 × 4 mm, 5 μm, Merck)] and reversed-phase [Kinetex C18 (150 × 4.6 mm, 5 μm, 100 Å, Phenomenex, Torrance, CA, USA) and Kinetex Phenyl-hexyl] columns. The flow rate was 1 mL/min, and the injection volume was 10 μL. The data were acquired and processed with Empower 3 and LabSolutions software 5.111. All solvents used for CC were of at least analytical grade (VWR Ltd., Szeged, Hungary). Ultrapure water was prepared with a Milli-Q water purification system (Millipore, Molsheim, France).

3.2. Plant Material

The whole plants of *Carex praecox* Schreb. (1.8 kg of dried plant material) were collected during the flowering period in Besenyőtelek, Hungary (GPS coordinates: 47.691670, 20.438270) in July 2019 and were identified by László Bakacsy (Department of Plant Biology, University of Szeged, 6726 Szeged, Hungary). A voucher specimen (No. 899) was deposited in the Herbarium of the Department of Pharmacognosy, University of Szeged, Szeged, Hungary.

3.3. Extraction and Isolation

The dried and ground whole *C. praecox* plant (1.8 kg) was percolated with methanol (MeOH, 50 L) at room temperature. The methanolic extract was concentrated in vacuo (310 g), dissolved in 50% aqueous methanol (1500 mL), and subjected to solvent–solvent partition with *n*-hexane (10 × 500 mL), chloroform ($CHCl_3$, 10 × 500 mL), and ethyl acetate (EtOAc, 10 × 500 mL).

The concentrated $CHCl_3$-soluble fraction (11 g) was further separated by the normal phase (NP) vacuum liquid chromatography (VLC) applying a gradient solvent system of $CHCl_3$–MeOH [from 100:0 to 8:2, and finally MeOH (500 mL/eluent)] resulting in 11 main fractions (C/A-K). Fraction C/B (354 mg) was further separated by a reversed-phase (RP) MPLC, affording 10 subfractions (C/B/1–10). From fraction C/B/1, compound **23** (1.4 mg) and from fraction C/B/7, compound **8** (3.8 mg) were isolated using an NP and RP preparative thin-layer chromatography (prep TLC), and by NP-HPLC. Fraction C/C (482 mg) was further purified by an RP flash chromatography (FC) to yield 12 subfractions (C/C/1–12). Fraction C/C/1 was chromatographed using RP-VLC, RP-prep TLC, and RP-HPLC methods to yield compounds **6** (3 mg), **7** (2.7 mg), **2** (1.6 mg), and **3** (1.5 mg), while subfraction C/C/4 was purified by an NP-prep TLC and afforded compounds **5** (18.7 mg) and **4** (2.8 mg). Fraction C/D (203 mg) was subjected to gel chromatography using Sephadex LH-20 gel as a stationary phase and a mixture of MeOH–CH_2CL_2 (1:1) as an eluent, which resulted in seven subfractions (C/D/1–7). Fraction C/D/4 was purified by RP-prep TLC and RP-HPLC, and compounds **19** (1.4 mg) and **20** (4.5 mg) were isolated, while fraction C/D/6 afforded compound **22** (4.6 mg). Fraction C/E (564 mg) was subjected to an RP-VLC, applying gradient elution with MeOH–H_2O [from 1:9 to 9:1, and finally MeOH (300 mL/eluent)], resulting in 8 subfractions (C/E/1–8). From fraction C/E/6, compounds **24** (4.1 mg) and **25** (2.4 mg) were isolated through RP- and NP-VLC and an NP-HPLC. Fraction C/F (710 mg) was separated by an RP-MPLC, providing 14 subfractions (C/F/1–14). Using the RP-HPLC (gradient elution with acetonitrile–H_2O), the purification of fraction C/F/2 afforded compound **21** (2.6 mg), while C/F/13 yielded compound **9** (4.0 mg).

The concentrated EtOAc-soluble fraction (10 g) was subjected to VLC on NP silica gel, with a gradient system of $CHCl_3$–MeOH [from 98:2 to 7:3, and finally MeOH (800 mL/eluent)], to yield 11 main fractions (E/A-K). Fractions E/B (77 mg), E/D (339 mg), E/F (538 mg), E/G (2020 mg), and E/H (526 mg) were separated by gel chromatography on the Sephadex LH-20 stationary phase using MeOH–CH_2Cl_2 (1:1) as an eluent, yielding 4 (E/B/1–4), 8 (E/D/1–8), 9 (E/F/1–9), 8 (E/G/1–8), and 8 (E/H/1–8) subfractions, respectively. From fraction E/B/3, compound **26** (1.2 mg) was isolated via RP-HPLC. Fraction E/D/6 was purified via RP-prep TLC and RP-HPLC, and compounds **11** (12.9 mg) and **12** (1.2 mg) were obtained, while fraction E/D/8 proved to be pure for compound **10** (25.0 mg). From fraction E/F/2, compound **1** (8.8 mg) was obtained by RP-prep TLC (MeOH–H_2O 6:4). Fraction E/F/7 was subjected to rotational planar chromatography (RPC) [gradient system of $CHCl_3$–MeOH from 99:1 to 7:3, and finally MeOH (100 mL/eluent)] affording 5 subfractions. After purification by RP-HPLC (MeOH–H_2O gradient system), fraction E/F/7/3 yielded compounds **13** (10.7 mg) and **14** (27.1 mg). From fraction E/F/7/4, compound **15** (5.9 mg) was isolated by RP-HPLC (MeOH–H_2O gradient system). Fraction E/H/6 was further purified by RP-prep TLC, and RP-HPLC to obtain compounds **17** (16.4 mg) and **18** (3.6 mg). Fraction E/I (1631 mg) was subjected to RP-VLC, applying MeOH–H_2O gradient elution [from 1:9 to 8:2, and finally MeOH (300 mL/eluent)] to afford 5 subfractions. After purification by RP-prep TLC (MeOH–H_2O 1:1), fraction E/I/3 yielded compound **16** (4.7 mg).

Carexine A (**1**): yellowish oil; $[\alpha]_D^{26}$ −6.0 (*c* 0.20, MeOH); ^{1}H and ^{13}C NMR data (CD_3OD, see Table 1); HRESIMS *m/z* 658.2711 $[M + NH_4]^+$ (calcd for $C_{30}H_{44}NO_{15}$ 658.2711), 663.2258 $[M + Na]^+$ (calcd for $C_{30}H_{40}O_{15}Na$ 663.2264).

Carexine B (**2**): white amorphous solid; $[\alpha]_D^{26}$−14.4 (*c* 0.05, MeOH); ^{1}H and ^{13}C NMR data (CD_3OD, see Table 2); HRESIMS *m/z* 403.1443 $[M - H]^-$ (calcd for $C_{21}H_{23}O_8$ 403.1441).

Carexine C (**3**): pale yellow amorphous solid; $[\alpha]_D^{26}$ +7.6 (*c* 0.05, MeOH); ^{1}H and ^{13}C NMR data (CD_3OD, see Table 2); HRESIMS *m/z* 403.1443 $[M - H]^-$ (calcd for $C_{21}H_{23}O_8$ 403.1441).

Carexine D (**4**): pale yellow amorphous solid; ^{1}H and ^{13}C NMR data (CD_3OD, see Table 3); HRESIMS *m/z* 329.1018 $[M + H]^+$ (calcd for $C_{18}H_{17}O_6$ 329.1020).

Carexine E (**5**): light brown amorphous solid; ^{1}H and ^{13}C NMR data (CD_3OD, see Table 3); HRESIMS *m/z* 315.0865 $[M + H]^+$ (calcd for $C_{17}H_{14}O_6$ 315.0869).

Compound **8** (*chrysosplenol F*): ^{1}H NMR (CD_3OD) δ_H 7.02 (1H, s, H-6′), 6.55 (1H, d, *J* = 2.2 Hz, H-8), 6.48 (1H, s, H-3′), 6.34 (1H, d, *J* = 2.2 Hz, H-6), 3.87 (3H, s, 7-OMe), 3.83 (3H, s, 5′-OMe), 3.74 (3H, s, 3-OMe); δ_C 180.0 (C-4), 167.3 (C-7), 162.9 (C-5), 159.2* (C-2), 159.0* (C-9), 152.3$^{\#}$ (C-2′), 152.1$^{\#}$ (C-4′), 142.8 (C-5′), 140.4 (C-3), 114.6 (C-6′), 109.1 (C-1′), 107.1 (C-10), 93.3 (C-8), 105.3 (C-3′), 99.0 (C-6), 56.5 (OMe-7), 57.3 (OMe-5′), 61.2 (OMe-3); *,$^{\#}$ are interchangeable.

Compound **9** (*tricin*): ^{1}H NMR (CD_3OD) δ_H 7.25 (2H, s, H-2′,6′), 6.63 (1H, s, H-3), 6.45 (1H, d, *J* = 2.0 Hz, H-8), 6.2 (1H, d, *J* = 2.0 Hz, H-6), 3.95 (6H, s, 2 × OMe, 3′,5′).

3.4. Pharmacological Assays

3.4.1. ACE-Inhibitory Assay

Angiotensin-converting enzyme inhibition was determined using the Angiotensin-I Converting Enzyme (ACE) Activity Assay Kit (CS0002, Sigma-Aldrich, USA) with modification of the volume of enzyme and samples added to the wells. In summary, a 96-well black plate (655096, F-bottom, Grenier bio-one, Frickenhausen, Germany) containing 25 µL of samples diluted in methanol-assay buffer was filled with 25 µL of enzyme solution (each 25 µL contained 1.5 mU of the ACE: ACE from rabbit lung, A6778, Sigma-Aldrich, USA). The solution was incubated for 5 min at 37 °C with shaking, and then 50 µL of the substrate (a 100-fold dilution of the substrate provided) was added. A plate reader (BMG Lambtech GmbH, Ortenberg, Germany) was used to monitor the fluorescence for 5 min in kinetic mode at Ex/Em 290/450 nm as soon as the substrate was added. At the end of the measurement, the percentage inhibition by each compound was calculated as follows:

$$\% \text{ inhibition} = (\text{values without samples} - \text{sample values})/(\text{values without samples}) \times 100. \quad (1)$$

Dose–effect studies on the compounds **12**–**18** were used to determine the concentration that inhibits 50% of the ACE. ACE-inhibitory kinetic studies were performed on compound **16**, the most potent compound, to determine its inhibition mechanism. Similarly, 25 µL of enzyme was added to plate wells containing 25 µL of several concentrations of compound **16** (0–10 µM). Following a 5 min incubation period at 37 °C, 50 µL of the substrate Abz-Gly-Phe (NO_2)-Pro (4003531, Bachem, Bubendorf, Switzerland) was added at varying concentrations (125–500 µM). The plate reader was then used to monitor the fluorescence in kinetic mode at extinction values of Ex/Em 290/450 nm. The Michaelis constant (Km) and maximal velocity (Vmax) of ACE were determined via Lineweaver–Burk plots, using the pharmacological and biochemistry transform and simple linear regression functions of the software, GraphPad Prism 8.0 (La Jolla, CA, USA).

3.4.2. Domain-Specific Studies

ACE domain-specific inhibition studies were performed based on previously reported methods (Carmona et al., 2006 [57]; Lunow et al., 2015 [58]). Fluorescence resonance energy transfer (FRET) substrates, Abz-SDK(Dnp)P-OH and Abz-LFK(Dnp)-OH were used for the N-domain and C-domain, respectively. The initial velocity of the reaction was determined using various concentrations (1–128 µM) of the FRET substrates. Briefly, 40 µL of assay buffer and 60 µL of the FRET substrate solutions were preincubated for 10 min at 37 °C, with the reaction started by adding 20 µL of diluted ACE solution (5 µL ACE + 15 µL 0.1 mol/L TRIS buffer) and fluorescence measured at λex/λem = 290/450 nm every minute at 37 °C for 30 min. The corresponding K_M of the FRET substrates, determined using the Michaelis–Menten equation, was used as the substrate concentration of the FRET substrates used in percent inhibition studies. The inhibitory activity of 16 on both domains was determined as described above with the 40 µL solution containing the inhibitor (inhibitor in DMSO–Assay buffer, 1:9). The control samples, which correspond to 100% enzyme activity, were prepared by replacing the inhibitor solution with TRIS buffer. Dose–effect studies on

16 using the FRET substrates were used to determine the IC_{50} of this compound on both ACE domains. All experiments were performed in triplicates. The ACE-inhibitory activity was calculated using the following equation:

$$(\%) = (Ab - Aa) - (Cb - Ca)/(Ab - Aa) \times 100 \quad (2)$$

where Aa is the absorbance of control wells at 0 min; Ab is the absorbance of control wells at 15 min; Ca is the absorbance of the inhibitor wells at 0 min; and Cb is the absorbance of inhibitor wells at 15 min.

3.4.3. Molecular Docking

The structure of the compound was drawn using a ChemDraw 12.0.2 software (ACD/LABS, Advanced Chemistry Development, Inc., Toronto, ON, Canada), and the energy of the compound (**16**) was minimized at the default mode, using a minimum RMS gradient of 0.010 in the software, Chem3D Pro 12.0 (ACD/LABS, Advanced Chemistry Development, Inc.). The energy-minimized compound was subsequently saved in PDB format before using it in the docking procedure. The X-ray crystallographic structures of the C- and N-domains of the human angiotensin I-converting enzyme complexed with lisinopril were obtained from the RCSB Protein Data Bank (PDB ID: 1O86 and 2C6N, respectively) [56,59]. PDB files for the enzyme and compounds were converted to the PDBQT format using the graphical user interface, AutoDock4 (The Scripps Research Institute, La Jolla, CA, USA) [60].

Before the docking analysis, water molecules and the lisinopril were eliminated from the 1O86 ACE protein model (C-domain) using AutoDock 4.2 (The Scripps Research Institute), while the zinc and chlorine atoms were retained in the ACE protein model, as these have been reported to be essential for the activity of ACE. By adding polar hydrogens, combining non-polar hydrogens, and adding Kollman charge to 1O86 using AutoDockTools, the final receptor for docking was created. A grid box (X: 43.817, Y: 38.308, and Z: 46.652, with 50 × 70 × 50 grid points of 0.375 Å spacing) created to include all active residues around the Zn(II) prosthetic group was used to calculate the zinc-centered map for ACE 1O86 [61].

The N-domain enzyme, 2C6N, was prepared using an identical method to the one used in preparing the C-domain enzyme, except that the protein's water molecules and sugar moieties were eliminated along with the lisinopril. To encompass all active residues and Zn(II) heteroatom in the A chain of this domain [62], a grid box (X: −28.034, Y: −24.612, and Z: −33.992; number of grid points in the three dimensions [npts]: X: 70, Y: 70, and Z: 60; spacing: 0.375 Å) was defined.

The docking procedure was performed with 10 docking runs. The Lamarckian algorithm was used to dock ligands once the docking parameters were set to their default settings. The binding energies were obtained from the resulting DLG files, and visualization of the interactions was achieved via Biovia (Discovery Studio visualizer version 21.1.0.20298; Dassault Systèmes, Vélizy-Villacoublay, France) after conversion of the docked PDBQT files into PDB files using OpenBabel GUI software version 2.4.1 [63].

3.4.4. Cell Line Cultures

Two human colon adenocarcinoma cell lines, namely Colo 205 (ATCC-CCL-222) doxorubicin-sensitive parent cells and Colo 320/MDR-LRP (ATCC-CCL-220.1) doxorubicin-resistant cells expressing ABCB1, were purchased from LGC Promochem (Teddington, UK). The cells were cultured in an RPMI-1640 medium supplemented with 10% heat-inactivated fetal bovine serum (FBS), 2 mM of L-glutamine, 1 mM of sodium pyruvate, and 100 mM of HEPES. The cells were incubated at 37 °C, in a 5% CO_2 and 95% air atmosphere.

3.4.5. Antiproliferative Assay

The antiproliferative effects of the compounds were tested in decreasing serial dilutions (2-fold dilutions starting from 100 μM) of human cancer cell lines (Colo 205, Colo 320) in

96-well flat-bottomed microtiter plates. First, the compounds were diluted in 100 µL of the medium, and then 6×10^3 cells in 100 µL of RPMI medium were added to each well, excluding the medium control wells. The culture plates were incubated at 37 °C for 72 h. Following incubation, 20 µL of the MTT solution (from a 5 mg/mL stock solution) was added to each well. After incubation at 37 °C for 4 h, 100 µL of sodium dodecyl sulfate (SDS) solution (10% SDS in 0.01 M HCl) was added to each well, and the plates were further incubated at 37 °C overnight. Cell growth was determined by measuring the optical density at 540 nm (ref.: 630 nm) using a Multiscan EX ELISA reader (Thermo Labsystems, Cheshire, WA, USA). The concentration that decreased cell viability by 50% was expressed as the IC_{50} (µM) ± SD for each compound, derived using the log (inhibitor) vs. response nonlinear fitting model of GraphPad Prism Version 9.4.0.

3.4.6. Bacterial Strains and Culture Conditions for Antimicrobial Assays

The test microorganisms included the standard Gram-positive strains *Staphylococcus aureus* (ATCC 29213), methicillin-resistant *S. aureus* (MRSA) (ATCC 43300), *S. epidermidis* (ATCC 12228), *Streptococcus pyogenes* (ATCC 19615), and *Bacillus subtilis* (ATCC 6633). The standard Gram-negative strains were *Escherichia coli* (ATCC 35218), *Klebsiella pneumoniae* (ATCC 700603), *Pseudomonas aeruginosa* (ATCC 27853), and *Moraxella catarrhalis* (ATCC 25238). The bacterial cultures were grown on a standard Mueller–Hinton (MH) agar at 37 °C overnight in an aerobic environment.

3.4.7. Determination of Antibacterial Activity Using the Disk Diffusion Method

The disk diffusion method was employed to screen compounds for their antibacterial activities against standard bacterial strains to determine their inhibitory zones. Briefly, the samples were dissolved in DMSO at a concentration of 10 mM. Sterile filter paper disks [6 mm in diameter, Whatman antibiotic paper disk (Cytiva, Marlborough, MA, USA)] coated with 10 µL of the sample solutions were placed on top of the bacterial suspension (inoculum: 0.5 McFarland, 1.5×10^8 CFU·mL^{-1}). The disks containing antibiotics (ciprofloxacin and ampicillin) were used as positive controls, and the disks containing DMSO served as negative controls. Under aerobic conditions, the plates were incubated at 37 °C for 20 h. The diameters of the zones of inhibition caused by the compounds, including the disk, were measured in triplicate. For each of the three repetitions, an average zone of inhibition was calculated [64].

4. Conclusions

The phytochemical investigation of a Hungarian sedge, *C. praecox*, resulted in the isolation and identification of 26 compounds, among which there are 5 new natural compounds, carexines A–E (**1**–**5**). Considering the chemical characteristics of the isolated compounds, the main constituents of *C. praecox* are phenolic compounds, mainly stilbenes (**12**–**18**). The ACE-inhibitory capacity of the isolated stilbenes was evaluated, the tetramer (–)-hopeaphenol (**16**) being the most potent inhibitor of the enzyme. The domain-specific assay revealed that hopeaphenol binds favorably to the N-domain of the ACE, which was also affirmed by the in silico docking studies. Selective inhibitors of the N-domain could be applied to treat tissue injury and fibrosis without affecting blood pressure and facilitate hematopoietic recovery after cancer chemotherapy.

Supplementary Materials: The following supporting information can be downloaded at: https://www.mdpi.com/article/10.3390/molecules29143427/s1, Figures S1–S73: 1D and 2D NMR, and HRESIMS spectra of compounds **1**–**5**, ^{1}H and JMOD spectra of **6**–**23**, and ^{1}H NMR spectra of **24**–**26**.

Author Contributions: Conceptualization, A.V.; methodology, A.V.; investigation, C.Z.D., N.K., R.B., A.K., G.S., and O.G.A.; resources, J.H.; data curation, A.V.; writing—original draft preparation, C.Z.D. and A.V.; writing—review and editing, J.H. and A.H.; supervision, A.V.; project administration, A.V.; funding acquisition, J.H. All authors have read and agreed to the published version of the manuscript.

Funding: This research was funded by the National Research, Development and Innovation Office, Hungary (NKFIH; K-135845 and K-134704), and the Ministry of Innovation and Technology of Hungary from NKFIH Fund, project no. TKP2021-EGA-32.

Institutional Review Board Statement: Not applicable.

Informed Consent Statement: Not applicable.

Data Availability Statement: The original contributions presented in the study are included in the article/Supplementary Materials, further inquiries can be directed to the corresponding author (A.V.).

Acknowledgments: Support from the New National Excellence Program of the Ministry of Human Capacities [UNKP-21-3 (C.Z.D.)] is gratefully acknowledged.

Conflicts of Interest: The authors declare no conflicts of interest. The funders had no role in the design of the study; in the collection, analyses, or interpretation of data; in the writing of the manuscript; or in the decision to publish the results.

References

1. WHO: The Top 10 Causes of Death. Available online: https://www.who.int/news-room/fact-sheets/detail/the-top-10-causes-of-death (accessed on 29 February 2024).
2. Curtin, S.C.; Tejada-Vera, B.; Bastian, B.A. Deaths: Leading causes for 2020. In *National Vital Statistics Reports*; National Center for Health Statistics: Hyattsville, MD, USA, 2023; Volume 72, No 13.
3. OECD: Main Causes of Mortality. Available online: https://www.oecd-ilibrary.org/sites/a72a34af-en/index.html?itemId=/content/component/a72a34af-en (accessed on 29 February 2024).
4. Bernstein, K.E.; Shen, X.Z.; Gonzalez-Villalobos, R.A.; Billet, S.; Okwan-Duodu, D.; Ong, F.S.; Fuchs, S. Different in vivo functions of the two catalytic domains of angiotensin-converting enzyme (ACE). *Curr. Opin. Pharmacol.* **2011**, *11*, 105–111. [CrossRef] [PubMed]
5. Masuyer, G.; Schwager, S.; Sturrock, E.; Isaac, R.E.; Acharya, K.R. Molecular recognition and regulation of human angiotensin-I converting enzyme (ACE) activity by natural inhibitory peptides. *Sci. Rep.* **2012**, *2*, 717. [CrossRef] [PubMed]
6. Alves-Lopes, R.; Montezano, A.C.; Neves, K.B.; Harvey, A.; Rios, F.J.; Skiba, D.S.; Arendse, L.B.; Guzik, T.J.; Graham, D.; Poglitsch, M.; et al. Selective inhibition of the C-domain of ACE (Angiotensin-Converting Enzyme) combined with inhibition of NEP (Neprilysin)—A potential new therapy for hypertension. *Hypertension* **2021**, *78*, 604–616. [CrossRef] [PubMed]
7. Fiorentino, A.; D'Abrosca, B.; Pacifico, S.; Izzo, A.; Letizia, M.; Esposito, A.; Monaco, P. Potential allelopatic effects of stilbenoids and flavonoids from leaves of *Carex distachya* Desf. *Biochem. Syst. Ecol.* **2008**, *36*, 691–698. [CrossRef]
8. Dhar, P.; Dhar, D.G.; Rawat, A.K.S.; Srivastava, S. Medicinal chemistry and biological potential of *Cyperus rotundus* Linn.: An overview to discover elite chemotype(s) for industrial use. *Ind. Crops Prod.* **2017**, *108*, 232–247. [CrossRef]
9. Cho, N.; Valenciano, A.L.; Du, Y.; Clement, J.; Cassera, M.B.; Goetz, M.; Kingston, D.G. Antiplasmodial flavanones and a stilbene from *Carpha glomerata*. *Bioorg. Med. Chem. Lett.* **2018**, *28*, 3368–3371. [CrossRef] [PubMed]
10. Nakajima, K.; Taguchi, H.; Endo, T.; Yosioka, I. The constituents of *Scirpus fluviatilis* (Torr). A. Gray. I. The structures of two new hydroxystilbene dimers, scirpusin A and B. *Chem. Pharm. Bull.* **1978**, *26*, 3050–3057. [CrossRef]
11. Gamal, M.A.; Hani, K.M.K.; Sameh, E.S.; Sabrin, I.R.M. A Review: Compounds isolated from *Cyperus* species (Part I): Phenolics and nitrogenous. *Int. J. Pharm. Phytochem. Res.* **2015**, *7*, 51–67.
12. Dávid, C.Z.; Hohmann, J.; Vasas, A. Chemistry and pharmacology of Cyperaceae stilbenoids: A review. *Molecules* **2021**, *26*, 2794. [CrossRef]
13. Fiorentino, A.; D'Abrosca, B.; Pacifico, S.; Natale, A.; Monaco, P. Structures of bioactive carexanes from the roots of *Carex distachya* Desf. *Phytochemistry* **2006**, *67*, 971–977. [CrossRef]
14. Kurihara, H.; Kawabata, J.; Ichikawa, S.; Mizutani, J. (–)-ε-Viniferin and related oligostilbenes from *Carex pumila* Thunb. (Cyperaceae). *Agric. Biol. Chem.* **1990**, *54*, 1097–1099. [CrossRef]
15. Arraki, K.; Richard, T.; Badoc, A.; Pédrot, E.; Bisson, J.; Waffo-Téguo, P.; Mahjoub, A.; Mérillon, J.M.; Decendit, A. Isolation, characterization and quantification of stilbenes from some *Carex* species. *Rec. Nat. Prod.* **2013**, *7*, 281–291.
16. Sotheeswaran, S.; Pasupathy, V. Distribution of resveratrol oligomers in plants. *Phytochemistry* **1993**, *32*, 1083–1092. [CrossRef]
17. Teka, T.; Zhang, L.; Ge, X.; Li, Y.; Han, L.; Yan, X. Stilbenes: Source plants, chemistry, biosynthesis, pharmacology, application and problems related to their clinical application—A comprehensive review. *Phytochemistry* **2022**, *197*, 113128. [CrossRef] [PubMed]
18. Matsushita, H.; Miyase, T.; Ueno, A. Lignan and terpene glycosides from *Epimedium sagittatum*. *Phytochemistry* **1991**, *30*, 2025–2027. [CrossRef]
19. Yamauchi, H.; Kakuda, R.; Yaoita, Y.; Machida, K.; Kikuchi, M. Two new glycosides from the whole plant of *Gleochoma hederacea* L. *Chem. Pharm. Bull.* **2007**, *55*, 346–347. [CrossRef] [PubMed]
20. In, S.J.; Seo, K.H.; Song, N.Y.; Lee, D.S.; Kim, Y.C.; Baek, N.I. Lignans and neolignans from the stems of *Viburnum erosum* and their neuroprotective and anti-inflammatory activity. *Arch. Pharm. Res.* **2015**, *38*, 26–34. [CrossRef] [PubMed]

21. Moon, S.S.; Rahman, A.A.; Kim, J.Y.; Kee, S.H. Hanultarin, a cytotoxic lignan as an inhibitor of actin cytoskeleton polymerization from the seeds of *Trichosanthes kirilowii*. *Bioorg. Med. Chem.* **2008**, *16*, 7264–7269. [CrossRef]
22. Xie, L.H.; Akao, T.; Hamasaki, K.; Deyama, T.; Hattori, M. Biotransformation of pinoresinol diglucoside to mammalian lignans by human intestinal microflora, and isolation of *Enterococcus faecalis* strain PDG-1 responsible for the transformation of (+)-pinoresinol to (+)-lariciresinol. *Chem. Pharm. Bull.* **2003**, *51*, 508–515. [CrossRef]
23. Arisawa, M.; Hayashi, T.; Shimizu, M.; Morita, N. Isolation and cytotoxicity of two new flavonoids from *Chrysosplenium grayanum* and related flavonols. *J. Nat. Prod.* **1991**, *54*, 898–901. [CrossRef]
24. Wang, Y.; Shen, J.Z.; Chan, Y.W.; Ho, W.S. Identification and growth inhibitory activity of the chemical constituents from *Imperata cylindrica* aerial part ethyl acetate extract. *Molecules* **2018**, *23*, 1807. [CrossRef] [PubMed]
25. Sinha, R.; Gadhwal, M.K.; Joshi, U.J.; Srivastava, S.; Govil, G. Modifying effect of quercetin on model biomembranes: Studied by molecular dynamic simulation, DSC and NMR. *Int. J. Curr. Pharm. Res.* **2012**, *4*, 70–79.
26. Ahmed, B.; Al-Howiriny, T.A. Two new hydroxy chalcone derivatives from *Thymus cilicicus*. *Z. Naturforsch B* **2007**, *62*, 121–124. [CrossRef]
27. Guiso, M.; Marra, C.; Farina, A. A new efficient resveratrol synthesis. *Tetrahedron Lett.* **2002**, *43*, 597–598. [CrossRef]
28. Kim, H.J.; Chang, E.J.; Bae, S.J.; Shim, S.M.; Park, H.D.; Rhee, C.H.; Park, J.H.; Choi, S.W. Cytotoxic and antimutagenic stilbenes from seeds of *Paeonia lactiflora*. *Arch. Pharm. Res.* **2002**, *25*, 293–299. [CrossRef]
29. Kurihara, H.; Kawabata, J.; Ichikawa, S.; Mishima, M.; Mizutani, J. Oligostilbenes from *Carex kobomugi*. *Phytochemistry* **1991**, *30*, 649–653. [CrossRef]
30. Aisha, F.; Din, L.B.; Yaacob, W.A. Resveratrol tetramer of hopeaphenol isolated from *Shorea johorensis* (Dipterocarpaceae). In Proceedings of the 2014 UKM FST Postgraduate Colloquium, Selangor, Malaysia, 9–11 April 2014; Volume 1614, pp. 302–308. [CrossRef]
31. Häusler, M.; Montag, A. Isolation, identification and quantitative determination of the norisoprenoid (S)-(+)-dehydrovomifoliol in honey. *Z. Lebensm. Unters. Forsch.* **1989**, *189*, 113–115. [CrossRef]
32. Yan, Z.H.; Han, Z.Z.; Hu, X.Q.; Liu, Q.X.; Zhang, W.D.; Liu, R.H.; Li, H.L. Chemical constituents of *Euonymus alatus*. *Chem. Nat. Compd.* **2013**, *49*, 340–342. [CrossRef]
33. Kataoka, K.I.; Shiota, T.; Takeyasu, T.; Mochizuki, T.; Taneda, K.; Ota, M.; Tanabe, H.; Yamaguchi, H. Potent inhibitors of acyl-CoA:cholesterol acyltransferase. Structure-activity relationships of novel N-(4-oxo-8-chromanyl) amides. *J. Med. Chem.* **1995**, *38*, 3174–3186. [CrossRef]
34. Pendse, R.; Rao, A.V.R.; Venkataraman, K. 5,7-Dihydroxychromone from *Arachis hypogoea* shells. *Phytochemistry* **1973**, *12*, 2033–2034. [CrossRef]
35. Suresh, D.; Gurudutt, K.N.; Srinivasan, K. Degradation of bioactive spice compound: Curcumin during domestic cooking. *Eur. Food Res. Technol.* **2008**, *228*, 807–812. [CrossRef]
36. Fishman, A.; Tao, Y.; Wood, T.K. Toluene 3-monooxygenase of *Ralstonia pickettii* PKO1 is a para-hydroxylating enzyme. *J. Bacteriol.* **2004**, *186*, 3117–3123. [CrossRef] [PubMed]
37. Sies, H. Polyphenols and health: Update and perspectives. *Arch. Biochem. Biophys.* **2010**, *501*, 2–5. [CrossRef]
38. Manach, C.; Scalbert, A.; Morand, C.; Rémésy, C.; Jiménez, L. Polyphenols: Food sources and bioavailability. *Am. J. Clin. Nutr.* **2004**, *79*, 727–747. [CrossRef] [PubMed]
39. Rudrapal, M.; Khairnar, S.J.; Khan, J.; Dukhyil, A.B.; Ansari, M.A.; Alomary, M.N.; Alshabrmi, F.M.; Palai, S.; Kumar, P.; Devi, R. Dietary polyphenols and their role in oxidative stress-induced human diseases: Insights into protective effects, antioxidant potentials and mechanism(s) of action. *Front. Pharmacol.* **2022**, *13*, 806470. [CrossRef] [PubMed]
40. Loupit, G.; Fonayet, J.V.; Lorensen, M.D.B.B.; Franc, C.; De Revel, G.; Janfelt, C.; Cookson, S.J. Tissue-specific stilbene accumulation is an early response to wounding/grafting as revealed by using spatial and temporal metabolomics. *Plant Cell Environ.* **2023**, *46*, 3871–3886. [CrossRef] [PubMed]
41. DellaGreca, M.; Cutillo, F.; D'Abrosca, B.; Fiorentino, A.; Zarrelli, A. Isolation of seed germination and plant growth inhibitors from mediterranean plants: Their potential use as herbicides. In *Natural Products for Pest Management*; Rimando, A.M., Duke, S.O., Eds.; American Chemical Society: New York, NY, USA, 2006; Volume 927, pp. 24–36. [CrossRef]
42. Spencer, G.F.; Tjarks, L.W. Germination inhibition by 5,7-dihydroxychromone, a flavonoid decomposition product. *J. Plant Growth Regul.* **1985**, *4*, 177–180. [CrossRef]
43. Tena, C.; Santiago, A.R.; Osuna, D.; Sosa, T. Phytotoxic activity of *p*-cresol, 2-phenylethanol and 3-phenyl-1-propanol, phenolic compounds present in *Cistus ladanifer* L. *Plants* **2021**, *10*, 1136. [CrossRef] [PubMed]
44. Kim, H.; Hwang, B.; Cho, S.; Kim, W.J.; Myung, S.C.; Choi, Y.H.; Kim, W.J.; Lee, S.; Moon, S.K. The ethanol extract of *Cyperus exaltatus* var. iwasakii exhibits cell cycle dysregulation, ERK1/2/p38 MAPK/AKT phosphorylation, and reduced MMP-9-mediated metastatic capacity in prostate cancer models in vitro and in vivo. *Phytomedicine* **2023**, *114*, 154794. [CrossRef]
45. Pagning, A.; Tamokou, J.D.D.; Lateef, M.; Tapondjou, L.; Kuiate, J.R.; Ngnokam, D.; Ali, M. New triterpene and new flavone glucoside from *Rhynchospora corymbosa* (Cyperaceae) with their antimicrobial, tyrosinase and butyrylcholinesterase inhibitory activities. *Phytochem. Lett.* **2016**, *16*, 121–128. [CrossRef]
46. Sayed, H.M.; Mohamed, M.H.; Farag, S.F.; Mohamed, G.A.; Proksch, P. A new steroid glycoside and furochromones from *Cyperus rotundus* L. *Nat. Prod. Res.* **2007**, *21*, 343–350. [CrossRef] [PubMed]

47. Santos, A.L.; Yamamoto, E.S.; Passero, L.F.D.; Laurenti, M.D.; Martins, L.F.; Lima, M.L.; Uemi, M.; Soares, M.G.; Lago, J.H.G.; Tempone, A.G.; et al. Antileishmanial activity and immunomodulatory effects of tricin isolated from leaves of *Casearia arborea* (Salicaceae). *Chem. Biodivers.* **2017**, *14*, e1600458. [CrossRef] [PubMed]
48. Kuwabara, H.; Mouri, K.; Otsuka, H.; Kasai, R.; Yamasaki, K. Tricin from a malagasy connaraceous plant with potent antihistaminic activity. *J. Nat. Prod.* **2003**, *66*, 1273–1275. [CrossRef] [PubMed]
49. Moon, J.; Park, S.; Jhee, K.; Yang, S. Protection against UVB-induced wrinkle formation in SKH-1 hairless mice: Efficacy of tricin isolated from enzyme-treated *Zizania latifolia* extract. *Molecules* **2018**, *23*, 2254. [CrossRef] [PubMed]
50. Coggon, P.; Janes, N.F.; King, F.E.; King, T.J.; Molyneux, R.J.; Morgan, J.W.W.; Sellars, K. Hopeaphenol, an extractive of the heartwood of *Hopea odorata* and *Balanocarpus heimii*. *J. Chem. Soc.* **1965**, 406–409. [CrossRef]
51. Tietjen, I.; Schonhofer, C.; Sciorillo, A.; Naidu, M.E.; Haq, Z.; Kannan, T.; Kossenkov, A.V.; Rivera-Ortiz, J.; Mounzer, K.; Hart, C.; et al. The natural stilbenoid (–)-hopeaphenol inhibits HIV transcription by targeting both PKC and NF-κB signaling and cyclin-dependent kinase 9. *Antimicrob. Agents Chemother.* **2023**, *67*, e01600-22. [CrossRef] [PubMed]
52. Tietjen, I.; Cassel, J.; Register, E.T.; Zhou, X.Y.; Messick, T.E.; Keeney, F.; Lu, L.D.; Beattie, K.D.; Rali, T.; Tebas, P.; et al. The natural stilbenoid (–)-hopeaphenol inhibits cellular entry of SARS-CoV-2 USA-WA1/2020, B.1.1.7, and B.1.351 variants. *Antimicrob. Agents Chemother.* **2021**, *65*, e0077221. [CrossRef]
53. Sharifi, N.; Khajeh, K.; Mahernia, S.; Balalaie, S.; Ataie, G.; Jahanbani, R.; Amanlou, M. Probing angiotensin converting enzyme (ACE) domain-dependent inhibition of onopordia, isolated from *Onopordon acanthium* L., using a continuous fluorescent assay. *Pharm. Sci.* **2018**, *24*, 31–37. [CrossRef]
54. Dive, V.; Cotton, J.; Yiotakis, A.; Michaud, A.; Vassiliou, S.; Jiracek, J.; Vazeux, G.; Chauvet, M.T.; Cuniasse, P.; Corvol, P. RXP 407, a phosphinic peptide, is a potent inhibitor of angiotensin I converting enzyme able to differentiate between its two active sites. *Proc. Natl. Acad. Sci. USA* **1999**, *96*, 4330–4335. [CrossRef]
55. Forli, S.; Huey, R.; Pique, M.E.; Sanner, M.F.; Goodsell, D.S.; Olson, A.J. Computational protein-ligand docking and virtual drug screening with the AutoDock suite. *Nat. Protoc.* **2016**, *11*, 905–919. [CrossRef]
56. Corradi, H.R.; Schwager, S.L.; Nchinda, A.T.; Sturrock, E.D.; Acharya, K.R. Crystal structure of the N domain of human somatic angiotensin I-converting enzyme provides a structural basis for domain-specific inhibitor design. *J. Mol. Biol.* **2006**, *357*, 964–974. [CrossRef] [PubMed]
57. Carmona, A.K.; Schwager, S.L.; Juliano, M.A.; Juliano, L.; Sturrock, E.D. A continuous fluorescence resonance energy transfer angiotensin I-converting enzyme assay. *Nat. Protoc.* **2006**, *1*, 1971–1976. [CrossRef]
58. Lunow, D.; Kaiser, S.; Rückriemen, J.; Pohl, C.; Henle, T. Tryptophan-containing dipeptides are C-domain selective inhibitors of angiotensin converting enzyme. *Food Chem.* **2015**, *166*, 596–602. [CrossRef] [PubMed]
59. Natesh, R.; Schwager, S.L.; Sturrock, E.D.; Acharya, K.R. Crystal structure of the human angiotensin-converting enzyme–lisinopril complex. *Nature* **2003**, *421*, 551–554. [CrossRef]
60. Morris, G.M.; Huey, R.; Lindstrom, W.; Sanner, M.F.; Belew, R.K.; Goodsell, D.S.; Olson, A.J. AutoDock4 and AutoDockTools4: Automated docking with selective receptor flexibility. *J. Comput. Chem.* **2009**, *30*, 2785–2791. [CrossRef]
61. Xie, D.; Du, L.; Lin, H.; Su, E.; Shen, Y.; Xie, J.; Wei, D. In vitro-in silico screening strategy and mechanism of angiotensin I-converting enzyme inhibitory peptides from α-lactalbumin. *LWT* **2022**, *156*, 112984. [CrossRef]
62. Douglas, R.G.; Sharma, R.K.; Masuyer, G.; Lubbe, L.; Zamora, I.; Acharya, K.R.; Chibale, K.; Sturrock, E.D. Fragment-based design for the development of N-domain-selective angiotensin-1-converting enzyme inhibitors. *Clin. Sci.* **2014**, *126*, 305–313. [CrossRef]
63. O'Boyle, N.M.; Banck, M.; James, C.A.; Morley, C.; Vandermeerch, T.; Hutchison, G.R. Open Babel: An open chemical toolbox. *J. Cheminform.* **2011**, *3*, 33. [CrossRef]
64. Ghazal, T.S.A.; Schelz, Z.; Vidács, L.; Szemerédi, N.; Veres, K.; Spengler, G.; Hohmann, J. Antimicrobial, multidrug resistance reversal and biofilm formation inhibitory effect of *Origanum majorana* extracts, essential oil and monoterpenes. *Plants* **2022**, *11*, 1432. [CrossRef]